2008 IEEE/RSJ International Conference on Intelligent Robots and Systems
Acropolis Convention Center
Nice, France, Sept, 22-26, 2008

A GPS and Laser-based Localization for Urban and Non-Urban Outdoor Environments

Matthias Hentschel, Oliver Wulf and Bernardo Wagner

***Abstract*— This paper introduces a localization based on GPS and laser measurements for urban and non-urban outdoor environments. In this approach, the GPS pose is Kalman filtered using wheel odometry and inertial data and tightly integrated into a Monte Carlo Localization based on 3D laser range data and a line feature reference map. By applying to this kind of sensor fusion, global localization as well as precise position tracking in close distance to buildings is enabled where only poor GPS observations are available. Following the description of the localization system, real world experiments demonstrate the functionality of the presented approach.**

I. Introduction

Robot localization is the problem of estimating the robot's position and orientation (pose) relative to its environment. This is one of the main requirements for autonomous mobile robots. During the recent years, many different solutions for the localization problem have been presented. In addition to SLAM [5], a widely-used approach is the probabilistic localization method, the Monte Carlo Localization (MCL). The advantage of this algorithm is the possibility to represent non-linearity and the ability to handle multiple hypotheses. MCL has been successfully tested within different environments and with a number of different sensors including 2D laser scanners [8], cameras [1] and omnidirectional cameras [2]. In [13], MCL was used for ground truth evaluation of large urban outdoor SLAM. However, as a world model is required for the Monte Carlo Localization this method is inapplicable in unstructured non-urban outdoor environments. In these environments, global pose estimation is enabled by GPS. By applying to precise satellite receiver technology like DGPS or RTK-GPS and sensor fusion with wheel odometry and inertial data, position errors of only a few centimeters are realizable. This has been tested in various non-urban outdoor applications [4] [6] [9]. In contrast to non-urban environment, the accuracy of GPS is limited in urban areas. With tall buildings and narrow streets, the visibility of the satellites is limited. Furthermore, errors due to multipath propagation of the satellite signals increase in urban environments. Figure 1 illustrates the GPS position fixes and the real position during an exemplary test run in urban environment. In the vicinity of tall buildings, the GPS error mainly caused by multipath propagation, sums up to 50m.

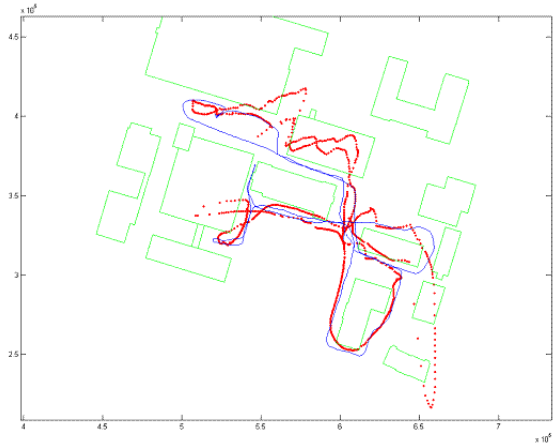

Fig. 1. Exemplary GPS position in urban outdoor environment (red line). The blue line represents the reference path. The outlines of buildings are labelled in green. The divergence between GPS and reference path is basically caused by multipath propagation errors.

Achieving a precise localization in urban as well as in non-urban environment, a combination of GPS and laser based localization is introduced in this paper. This approach consists of two steps. In the first step, the received GPS position fix is Kalman filtered with wheel odometry and inertial measurement data. Odometry and inertial data supplies outputs of low noise that slowly drift off over time. GPS has minimal drift but much more noise. The Kalman filter, using statistical models of both systems, can take advantage of their different error characteristics to improve the GPS position accuracy. Additionally, this GPS dead reckoning is able to bypass short-term GPS outtakes.

In the second step, the Kalman filtered GPS pose is integrated into a Monte Carlo Localization based on 3D laser range scans. The landmark information is extracted from the 3D point cloud using the method of *Virtual 2D Scans* [12]. For the world model, a simplified 2D line feature map is utilized containing static landmarks. The GPS pose is integrated into MCL by adding a (small) number of samples drawn from a Gaussian distribution centered at the Kalman filtered GPS position. Standard deviation of the distribution is the estimated uncertainty of the filtered GPS measurement. Additionally, the importance factors of the belief are adjusted according to the quality of the GPS measurement.

Matthias Hentschel, Oliver Wulf and Bernardo Wager are with the Real Time Systems Group (RTS) of the Institute for Systems Engineering, Leibniz Universität Hannover, Hannover, Germanry. E-mail: {hentschel, wulf, wagner}@rts.uni-hannover.de

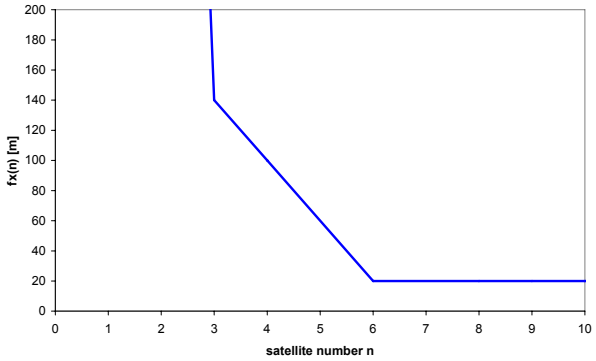

Fig. 2. Typical developing of $f_x(n)$ for estimating the measurement uncertainty of the x-component of the GPS position. If less than three satellites are available, $f_x(n)$ is defined as infinite.

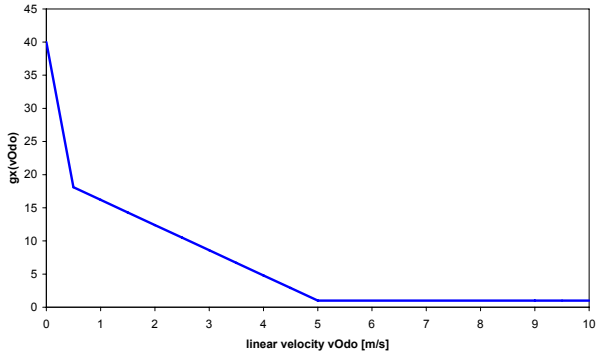

Fig. 3. Typical developing of the weighting function $g_x(v_{Odo})$ to consider the dependence of subsequent GPS measurements at low speeds.

Following the description of the GPS dead reckoning in Section II, the laser-based localization is presented in Section III. Finally, real-world experimental results are presented in Section IV.

II. GPS Dead Reckoning

A. GPS Measurement

The *Global Positioning System* GPS enables determination of position, speed, direction and time worldwide. A typical GPS receiver calculates its position by measuring the transit time and the data transmitted with the signals from at least four GPS satellites. The reference system for the position is the *World Geodetic System* (WGS84). Within this reference frame, the position is defined by its latitude, longitude and elevation above the reference ellipsoid. Nevertheless, for a fusion with odometry and inertial observations the position vector in radians is unsuitable. Therefore, the GPS position is transferred to a planar Cartesian reference frame like the *Universal Transverse Mercator* (UTM) or the *Gauss-Krueger* coordinate system. As most maps in Germany are referenced in the *Gauss-Krueger* coordinate system, this reference frame is used in this paper. Equation (1) shows the resulting measurement vector $\underline{z}_{k,Gps}$ of the GPS sensor at a discrete time k, transferred to the *Gauss-Krueger* coordinate system.

$$\underline{z}_{k,Gps} = \left(x_{Gps}, y_{Gps}, z_{Gps}, \rho_{Gps}\right)^T \tag{1}$$

The position on the surface of the reference ellipsoid is defined by x_{Gps} and y_{Gps} where x_{Gps} denotes the northing, the projected distance of the GPS position from the equator. The easting is denoted as y_{Gps}, which is the projected distance of the position from the central meridian. The elevation above the reference ellipsoid is defined by z_{Gps} and the robot orientation on the tangential plane on earth by ρ_{Gps}. The robot orientation is calculated using the difference between two subsequent GPS positions assuming only longitudinal movement of the robot. Associated with the GPS measurement vector $\underline{z}_{k,Gps}$ the measurement uncertainty is estimated as follows:

$$\underline{\sigma}_{k,Gps} = \left(\sigma_x, \sigma_y, \sigma_z, \sigma_\rho\right)^T \tag{2}$$

where σ_x and σ_y define the standard deviation of the position on the surface on the reference ellipsoid in x and y direction. The standard deviation of the elevation above the surface is denoted as σ_z and σ_ρ defining the standard deviation of the orientation. The estimated measurement uncertainty of the GPS is a product of the two function $f(n)$ and $g(v_{Odo})$

$$\underline{\sigma}_{k,Gps} = \begin{pmatrix} \sigma_x \\ \sigma_y \\ \sigma_z \\ \sigma_\rho \end{pmatrix} = \begin{pmatrix} f_x(n) \cdot g_x(v_{Odo}) \\ f_y(n) \cdot g_y(v_{Odo}) \\ f_z(n) \cdot g_z(v_{Odo}) \\ f_\rho(n) \cdot g_\rho(v_{Odo}) \end{pmatrix} \tag{3}$$

with n defining the number of satellites used for the position fix and v_{Odo} denoting the linear velocity of the robot based on wheel odometry measurements. The function $f(n)$ represents a generous estimate for the uncertainty caused by the geometric satellite constellation, atmospheric disturbances, multipath propagation and receiver noise. With increasing number of different satellite signals used for computing the position fix, the uncertainty decreases. As at least three satellites are required for computing a position fix, the uncertainty is assumed as infinite for less than three satellites. When the vehicle is operated at a slow velocity, the environmental conditions change only slightly between subsequent GPS measurements. As a result, subsequent GPS measurements are not fully independent. This is considered

by the second function $g(v_{Odo})$ which multiplies the uncertainty in dependence of the velocity v_{Odo}. Exemplified by Figure 2 and Figure 3, the function $f_{xy}(n)$ and $g_{xy}(v_{Odo})$ for a typical GPS receiver without differential corrections are displayed.

B. Kalman Filtering

Based on the GPS measurement vector $\underline{z}_{k,Gps}$ and the uncertainty estimation $\underline{\sigma}_{k,Gps}$ a sensor fusion with odometry an inertial measurement data is proposed by using a Kalman filter [3]. The Kalman filter consists of two steps, the measurement update (correction) and the time update (prediction). Detailed information about the theoretical background of Kalman filtering can be found in [10] and will not be explained here.

In the measurement update, the Kalman gain K_k is computed accordingly to

$$K_k = P_k^- H_k^T \left(H_k P_k^- H_k^T + R_k\right)^{-1} \tag{4}$$

where P_k^- is the predicted error estimation covariance and R_k is the measurement noise covariance. Following the estimated GPS measurement uncertainty in (3), the resulting measurement noise covariance for Kalman filtering the GPS measurement vector $\underline{z}_{k,Gps}$ is defined as

$$R_k = \left(\sigma_x, \sigma_y, \sigma_z, \sigma_\rho\right)^T \tag{5}$$

By inserting (5) and (14) in (4), the Kalman gain K_k is computed. Mapping the state vector $\underline{x}_k$ to the measurement $\underline{z}_{k,Gps}$, the observation matrix H_k is an identity matrix.

$$K_k = \begin{bmatrix} k_x & 0 & 0 & 0 \\ 0 & k_y & 0 & 0 \\ 0 & 0 & k_z & 0 \\ 0 & 0 & 0 & k_\rho \end{bmatrix} \tag{6}$$

$$K_k = \begin{bmatrix} \frac{p_x^-}{p_x^- + \sigma_x} & 0 & 0 & 0 \\ 0 & \frac{p_y^-}{p_y^- + \sigma_y} & 0 & 0 \\ 0 & 0 & \frac{p_z^-}{p_z^- + \sigma_z} & 0 \\ 0 & 0 & 0 & \frac{p_\rho^-}{p_\rho^- + \sigma_\rho} \end{bmatrix} \tag{7}$$

Based on the predicted state vector $\underline{x}_k^-$ the posteriori state vector is corrected using the current GPS observations

$$\underline{x}_k = \underline{x}_k^- + K_k\left(\underline{z}_{k,Gps} - H_k \underline{x}_k^-\right) \tag{8}$$

$$\underline{x}_k = \begin{pmatrix} x \\ y \\ z \\ \rho \end{pmatrix} = \begin{pmatrix} x^- + k_x\left(x_{Gps} - x^-\right) \\ y^- + k_y\left(y_{Gps} - y^-\right) \\ z^- + k_z\left(z_{Gps} - z^-\right) \\ \rho^- + k_\rho\left(\rho_{Gps} - \rho^-\right) \end{pmatrix} \tag{9}$$

Completing the measurement update, the covariance matrix is corrected with the Kalman gain K_k and the predicted error estimation covariance P_k^-.

$$P_k = \left(1 - K_k\right) P_k^- \tag{10}$$

$$P_k = \begin{pmatrix} p_x \\ p_y \\ p_z \\ p_\rho \end{pmatrix} = \begin{pmatrix} \frac{1-k_x}{p_x^-} \\ \frac{1-k_y}{p_y^-} \\ \frac{1-k_z}{p_z^-} \\ \frac{1-k_\rho}{p_\rho^-} \end{pmatrix} \tag{11}$$

In the prediction step, the a priori value of the state vector $\underline{x}_{k+1}^-$ is predicted using wheel odometry data.

$$\underline{x}_{k+1}^- = A_k \underline{x}_k = \begin{pmatrix} x^- \\ y^- \\ z^- \\ \rho^- \end{pmatrix} = \begin{pmatrix} x + \Delta x_{Odo} \\ y + \Delta y_{Odo} \\ z + \Delta z_{Odo} \\ \rho + \Delta \rho_{Odo} \end{pmatrix} \tag{12}$$

The components Δx_{Odo}, Δy_{Odo} and Δz_{Odo} represent the difference of position and $\Delta \rho_{Odo}$ the difference of orientation between the previous time step $k-1$ and k. These are measured by wheel odometry data transferred to the identical global reference frame of the GPS. When inertial sensor data is available, the wheel odometry and the gyro measurements are fused and inserted instead in (12).

Finally, the error estimation covariance is predicted for the next time step.

$$P_{k+1}^- = A_k P_k A_k^T + Q_k \tag{13}$$

$$P_{k+1}^{-} = \begin{pmatrix} p_x^- \\ p_y^- \\ p_z^- \\ p_\rho^- \end{pmatrix} = \begin{pmatrix} p_x \\ p_x \\ p_z \\ p_\rho \end{pmatrix} + \begin{pmatrix} \varepsilon_x \cdot \Delta d_{Odo} \\ \varepsilon_y \cdot \Delta d_{Odo} \\ \varepsilon_z \cdot \Delta d_{Odo} \\ \varepsilon_\rho \cdot \Delta d_{Odo} \end{pmatrix} \quad (14)$$

Using wheel odometry measurements, the covariance of dynamic disturbance noise is depending on the Euclidian distance Δd_{Odo} between the position at time step $k-1$ and k and a scalar noise constant ε. Dependent on the odometry drift, typical noise values are $\varepsilon_x = \varepsilon_y = \varepsilon_z = 0.1m/m$ and $\varepsilon_\rho = 1°/m$. Equation (15) shows the resulting measurement vector $\underline{z}_{k,Kal}$ of the Kalman filtered GPS observation at time k in the *Gauss-Krueger* coordinate system.

$$\underline{z}_{k,Kal} = \left(x_{Kal}, y_{Kal}, z_{Kal}, \rho_{Kal}\right)^T = \underline{x}_k \quad (15)$$

Related to the measurement vector, the Kalman filtered uncertainty is given by

$$\underline{\sigma}_{k,Kal} = \left(p_x, p_y, p_z, p_\rho\right)^T \quad (16)$$

III. Laser Based Localization

A. Monte Carlo Localization

Monte Carlo Localization (MCL) or particle filtering is a recursive Bayes filter that estimates the posteriori belief distribution of a robot's pose given a map of the environment and sensor data of motion and perception. Following [8], the belief $Bel(s)$ is represented by a set of n weighted samples (or particles) distributed according to $Bel(s)$:

$$Bel(s) \approx \left\{s^{(i)}, w^{(i)}\right\}_{i=1,\ldots,n} \quad (17)$$

where each $s^{(i)}$ is a sample of the random variable s, the hypothesized position and orientation of the robot. The importance (or weight) of each sample is determined by the non-negative numeric parameter $w^{(i)}$ called *importance factor* which represents the probability of being at the location. The recursive update of the basic MCL is realized in the following steps:

1. Resampling: draw a random sample s_{k-1} from the current belief, with a likelihood given by the importance factors of the belief $Bel(s_{k-1})$.
2. Predict: for this sample s_{k-1}, predict a successor pose s_k, according to the motion model $p(s_k \mid s_{k-1}, a_{k-1}, m)$.
3. Update: assign a preliminary (non-normalized) importance factor $p(o_k \mid s_k, m)$ to this sample and add it to the new sample set representing $Bel(s_k)$.
4. Repeat step 1 through 3 n times. Finally, normalize the importance factors in the new sample set $Bel(s_k)$ that they sum up to 1.

Following each recursive update, an estimate for the current pose of the robot is generated by averaging the best 10% samples in the current belief.

The initial belief $Bel(s_0)$ is a set of samples drawn from a narrow Gaussian distribution centered on the (known) start position of the robot, where each sample has the uniform initial weight n^{-1}.

For the world model, a simplified 2D line feature map representation is utilized containing only static landmarks. In the update step of the MCL, the map is used to calculate the expected range measurements (circular 2D scans) at a given pose. Using a sensor model described in [7], these range measurements are compared to the actual range measurements (*Virtual 2D Scans* [12] from the 3D laser scanner system) to determine the importance factor of the samples.

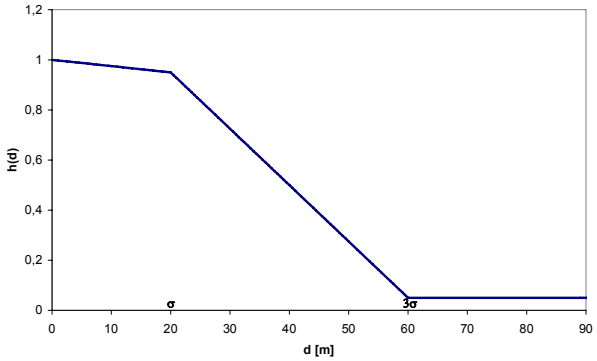

Fig. 4. Non-linear function $h(d)$ for adjusting the importance factors of the samples in dependence of the Euclidian distance d between samples and filtered GPS position.

B. GPS Integration

The Kalman filtered GPS observation $\underline{z}_{k,Kal}$ is integrated into the Monte Carlo Localization by the following steps:

A. Adjust the importance factors of all n samples in dependence of the Euclidian distance between samples s_k and the filtered GPS observation $\underline{z}_{k,Kal}$.
B. Draw a subset of m samples from a Gaussian distribution centered at the filtered GPS position $\underline{z}_{k,Kal}$ .and the standard deviation $\underline{\sigma}_{k,Kal}$ of the

filtered GPS position.

C. Add the subset of m GPS samples to the sample set representing $Bel(s_k)$ by replacing m samples with the lowest weight.

If the GPS uncertainty is below a certain threshold, the steps above are performed with each recursive update of the laser-based MCL.

Step A, the adjustment of the importance factors of the belief $Bel(s_k)$, is done in the Update (step 3) of the sample set in the basic MCL. By multiplying the importance factor $w^{(i)}$ with a non-linear function $h(d^{(i)})$, the weight is reduced in dependence of the distance d between the sample position $s_k^{(i)}$ and the filtered GPS position $\underline{z}_{k,Kal}$.

$$w^{(i)} = w^{(i)} \cdot h(d^{(i)}) \tag{18}$$

An exemplary function $h(d)$ is displayed in Figure 4. By adjusting the importance factors, the influences of outliers are reduced. Furthermore, the effect of hopping between multiple pose hypotheses of equal likelihood is reduced.

Step B and C are performed after Resampling (step 1) in the basic MCL. A number of m samples with the lowest weight in the belief $Bel(s_k)$ are replaced by a subset of Gaussian distributed samples. The subset is centered at the Kalman filtered GPS position with a standard deviation of $\underline{\sigma}_{k,Kal}$.

Finally, Figure 5 gives an overview of the GPS and laser-based localization presented in this paper. The resultant pose estimate is denoted as

$$\underline{z}_{k,Mcl} = (x_{Mcl}, y_{Mcl}, z_{Mcl}, \rho_{Mcl})^T \tag{19}$$

As MCL is two dimensional, note that z_{Mcl} is the Kalman filtered GPS elevation.

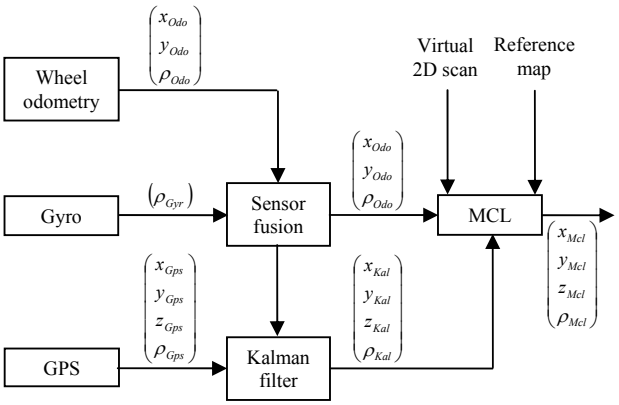

Fig. 5. Block diagram of the GPS- and laser-based localization.

IV. Experimental Results

A. Experimental Setup

The presented experiments have been carried out at a test site in northern Germany. This area includes urban environment with a maximum building height 10 m and non-urban environments as well. The experimental robot platform was manually driven on a path of 950 m length. The path starts from *S* and ends at the point labelled with *E* (see Figure 6). On this path, the maximum robot speed was 6 km/h and the average speed about 4km/h. For environmental perception, our custom-build *RTS ScanDrive* 3D laser sensor [11] was used. With an update rate of 0.4 Hz, the continuously rotating 3D scanner measures an overall number of 380 full 3D scans along the path. The maximum range of this sensor is 30m. Wheel odometry data is available with a data rate of 10 Hz. For the position fixes, a low-cost *Navilock NL303* GPS receiver with a *SiRF III* chip set was used. The update rate is 1 Hz and the position accuracy given by the manufacturer is 10m RMS. During the test run, at least 9 satellites were visible all the time. All required algorithms for the localization as well as data acquisition are computed in real-time using an Pentium III 700 MHz embedded PC with Linux/Xenomai real-time operating system onboard the robot. For evaluation, all processed data is logged as well.

The reference map used for this approach is based on a map from the German land registration office. This so-called "Automatisierte Liegenschaftskarte (ALK)" is a vector format containing lines that represent the outer walls of solid buildings. Each line is represented by two points in northing and easting coordinates in the Gauss-Krueger coordinate system. Buildings which were not included in the ALK were added manually by using a geo referenced aerial photograph. This section of the reference map contains 25 buildings which are represented by 233 line segments. The accuracy of the reference map is 0.5m.

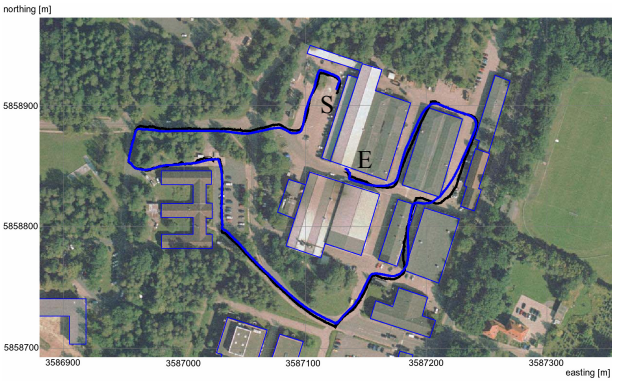

Fig. 6. GPS position (black line) and Kalman filtered GPS positon (blue line) of the experimental test run. The test run start at *S* and ends at the point labelled with *E*.

The particle filter used in the presented localization approach uses 200 samples and a generous estimate of the

sensor variance of 1m. This estimate includes the sensor range error, errors from scanning while moving and map uncertainties. Ten percent of the samples are distributed according to the Kalman filtered GPS measurement.

B. *Localization Results*

Figure 6 illustrates the localization results of the Kalman filtered GPS position. Marked with the black line, the raw GPS measurement is displayed. The blue line illustrates the results after Kalman filtering the GPS measurements with wheel odometry data. In the vicinity of building, the GPS position error highly increases, mainly caused by multipath propagation error. As the number of satellites used for the position fixes remains continuously above 9 satellites and the PDOP (Positional Dilution of Precision) value between 1.3 and 1.6, these errors are not directly determinable.

In these environments the position error can be reduced by the combination with a laser based localization as presented in this paper. The resultant particle filtered position is illustrated in Figure 7 by the red line. The blue line represents the Kalman filtered GPS measurement. Starting at the area marked with S, the robot localizes itself initially by GPS. For the following 80m of path length, the position is tracked using a combination of Kalman filtered GPS and laser based localization. As the distance to landmarks included in the reference map increases, the importance of the GPS samples rises. As a result, the filtered position fades towards the Kalman filtered GPS position when no landmarks are available. When landmarks are perceived again, the importance of the GPS samples decreases and the position is computed as the optimum between GPS and laser based localization. Thereby, the position accuracy increases highly especially in close distance to buildings. At the end of the test run, the robot is driven inside one of the buildings. As there is no clear view to the sky available, insufficient GPS signals are available for a position fix. However, the robot is still correctly localized by its laser based localization.

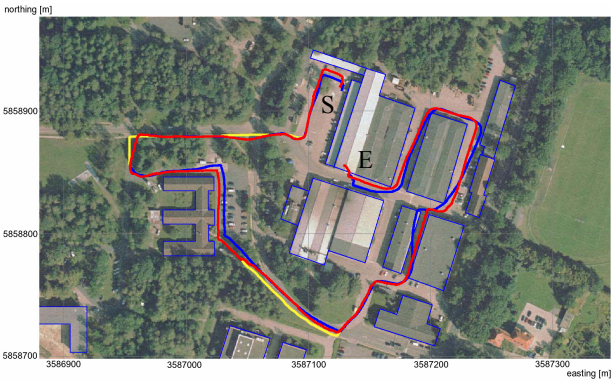

Fig. 7. Kalman filtered GPS position (blue line) and position from Monte Carlo Localization (red line). The actual robot path is indicated in yellow if different from the Monte Carlo Localization. Thin blue lines mark line features of the reference map used for MCL. The test run starts at *S* and ends at the point labelled with *E*.

For ground truth evaluation, the scan-data was manually monitored in areas where landmarks are available [13] during the test run.

V. Conclusion

This paper presents a novel approach for robot localization in urban as well as non-urban outdoor environments. In this approach, the GPS pose is Kalman filtered with wheel odometry and inertial data and directly integrated into a Monte Carlo Localization. Environmental perception is based on a 3D laser range sensor. The 3D point cloud is reduced to a *Virtual 2D Scan*, including mainly landmark information. For the world model, a simplified 2D line feature map is used containing static landmarks e.g. walls. Experimental results show that this approach enables a precise localization in urban and non-urban environments in real-time.

As the GPS samples are distributed within the Monte Carlo Localization with the Kalman filtered error covariance, the quality of the resultant pose is dependant of the estimated standard deviation of the GPS receiver. Future work will focus on the improvement of the GPS error estimation by using environmental information for estimating the GPS multipath propagation error.

References

[1] D. Fox, W. Burgard, F. Dellaert and S. Thrun, "Monte Carlo Localization: Efficient Position Estimation for Mobile Robots", in American Association for Artificial Intelligence, 1999.

[2] H. Gross, A. Koenig, H. Boehme and C. Schroeter, „Vision based Monte Carlo Self-Localization for a Mobile Service Robot Acting as Shopping Assistant in a Home Store", in International Conference on Intelligent Robots and Systems (ICRA), Lausanne, Switzerland, 2002.

[3] R. E. Kalman, "A New Approach to Linear Filtering and Prediction Problems", in *Transactions of the ASME – Journal of Basic Engineering*, 1960.

[4] A. Kelly et. al., "Towards Reliable Off Road Autonomous Vehicles Operating in Challenging Environments" in International Journal of Robotics Research, vol. 25, 2006.

[5] S. Kolski, D. Ferguson, M. Bellino and R. Siegwart, "Autonomous Driving in Structured and Unstructured Environments", in *IEEE Intelligent Vehicles Symposium*, 2006.

[6] N. Schmitz, J. Koch, M. Proetzsch and K. Berns, „Fault-Tolerant 3D Localization for Outdoor Vehicles", in International Conference on Intelligent Robots and Systems (IROS), 2006.

[7] S. Thrun, "Probabilistic Algorithms in Robotics", in *AI Magazine*, vol. 21 (4), 2000.

[8] S. Thrun, D.Fox, W. Burgard and F. Dellaert, "Robust Monte Carlo Localization for Mobile Robots", in Artificial Intelligence, vol. 128, 2001.

[9] S. Thrun et. Al., "Stanley, the Robot That Won the DARPA Grand Challenge", in Journal of Field Robotics, 2006.

[10] G. Welch and G. Bishop, "An Introduction to the Kalman Filter", in Kalman

[11] O. Wulf, and B. Wagner, "Fast 3D-Scanning Methods for Laser Measurement Systems", in *International Conference on Control Systems and Computer Science*, 2003.

[12] O. Wulf, K. O. Arras, H. I. Christensen and B. Wagner, "2D Mapping of Cluttered Indoor Environments by Means of 3D Perception", in *International Conference on Robotics and Automation (ICRA)*, 2004.

[13] O. Wulf, A. Nuechter, J. Hertzberg and B. Wagner, "Ground truth evaluation of Large Urban 6D SLAM", in International Conference on Intelligent Robots and Systems (IROS), 2007.